Available online at www.sciencedirect.com
SCIENCE DIRECT®
ELSEVIER
Linear Algebra and its Applications 380 (2004) 107–124
LINEAR ALGEBRA AND ITS APPLICATIONS
www.elsevier.com/locate/laa

A unified approach to fast image registration and a new curvature based registration technique

Bernd Fischer*, Jan Modersitzki

Institute of Mathematics, Medical University of Lübeck, 23560 Lübeck, Germany

Received 26 March 2002; accepted 1 October 2003

Submitted by R. Nabben

Abstract

Image registration is central to many challenges in medical imaging today. It has a vast range of applications.

The purpose of this note is twofold. First, we review some of the most promising non-linear registration strategies currently used in medical imaging. We show that all these techniques may be phrased in terms of a variational problem and allow for a unified treatment.

Second, we introduce, within the variational framework, a new non-linear registration model based on a curvature type smoother. We show that affine linear transformations belong to the kernel of this regularizer. As a result, the approach becomes more robust against poor initializations of a pre-registration step. Furthermore, we develop a stable and fast implementation of the new scheme based on a real discrete cosine transformation. We demonstrate the advantages of the new technique for synthetic data sets and present an application of the algorithm for registering MR-mammography images.

Keywords: Image registration; Variational approach; Fast linear solvers

1. Introduction

Image registration is an often encountered problem in many application areas like, for example, geophysics, medicine, and robotics. For an overview we refer to [6,20,21,34], and references therein.

* Corresponding author.
E-mail addresses: fischer@math.mu-luebeck.de (B. Fischer), modersitzki@math.mu-luebeck.de (J. Modersitzki).

0024-3795/$ - see front matter
doi:10.1016/j.laa.2003.10.021

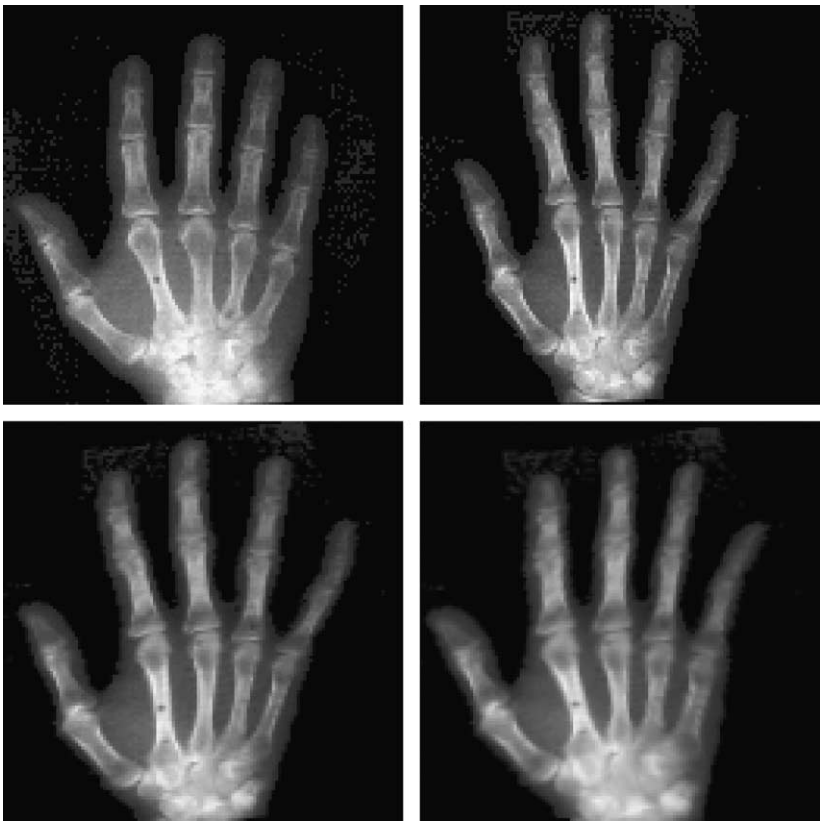

Fig. 1. Registration results for X-rays of a human hand (images from [1]). Top left: reference R, top right: template T, bottom left: template T^{LR} after affine linear registration, $||T^{\mathrm{LR}} - R||/||T - R|| = 65.5\%$, and bottom right: template T^{curv} after curvature registration, $||T^{\mathrm{curv}} - R||/||T - R|| = 37.6\%$.

Here, we focus on medical applications. In the last two decades, computerized image registration has played an increasingly important role in medical imaging. Registered images are now used routinely in a multitude of different applications, such as the treatment verification of pre- and post-intervention images and the time evolution of an agent injection subject to patient motion. They are also useful to take full advantage of the complementary information coming from multimodal imagery, like, for example, computer tomography (CT) and magnetic resonance imaging (MRI).

Applications of i.r.

The registration task is illustrated by the example depicted in Fig. 1. Given are two images, typically called *reference* R and *template* T. The goal is to find a spatial transformation, such that the deformed template matches the reference image subject to a suitable distance measure. In this example, we first compute an affine linear mapping such that the pointwise difference, also called *sum of squared differences*, between the images is as small as possible. The result of this scheme is shown in the

bottom left picture. Its difference to the given reference is reduced by about 35%. This so-called *linear matching* approach might be satisfying for some applications, but clearly not for all. Actually, often just a simple *rigid matching*, i.e. a translation and rotation of one image, is employed. Finally, the bottom right picture displays the result of a *non-linear matching* strategy, which will be discussed in detail in Section 4. Here the difference is reduced by another 30%.

Due to the wide range of applications a variety of different registration techniques have been developed (see, [20] for an overview, [19] for a connection to optical flow problems, and [22] for a very general treatment). Here, we focus on so-called *intensity-driven approaches*. These schemes aim to match intensity pattern between the deforming scan and the target based on mathematical or statistical criteria, like in Fig. 1. Interestingly, but widely unknown, most of these schemes allow for a variational formulation of the registration problem. Here, the functional to be minimized has two building blocks. One of them computes *internal forces*, which are defined for the wanted *displacement field* itself, whereas the other one is responsible for *external forces*, which are computed from the image data. The internal forces are designed to keep the displacement field smooth during deformation. The external forces are defined to obtain the desired registration result. The actual choice of the forces depends on the application under consideration and will be discussed in Section 2 for the most common choices.

The data, i.e. the reference and template images, come into play only in external forces

Internal forces used to make the displacement function sufficiently smooth

Many application may also demand for additional constraints, like for example, mass or volume preserving maps; cf., e.g., [16] or [25]. A treatment of these type of constraints in a variational setting is presented in [15]; for point to point relations see [14].

Non-linear schemes, sometimes also called *elastic matching* methods, are known to produce very satisfactory results. However, there are several problems with such fully automatic registration approaches. One of which is the fact that these schemes are computationally intensive. The original implementations had been rather slow which made them practically useless for real life applications. In the meantime there have been various attempts to come up with fast algorithms, see for example [4,11,12]. Another problem is that these techniques are sensitive to initial positioning of the images to be matched. If the initial linear alignment is off by too much, the non-linear matching procedure may perform poorly, i.e., does not converge to the wanted result. Therefore, a satisfying pre-registration step can be a key issue.

In this note we present a novel registration technique. Here, the internal forces are designed to minimize the curvature of the displacement field. For this *curvature registration* scheme, the internal forces not only provide smooth solutions but also allows for automatic affine linear alignment. As a consequence, a pre-registration step is not necessary. In conjunction with other registration procedures, the core step of the curvature registration requires the solution of a highly structured but very large linear system. Here, we design a fast and stable direct solver for the underlying system. The backbone is a real discrete cosine transformation (DCT) which results in an $\mathcal{O}(n \log n)$ implementation, where n is the number of voxel.

The paper is organized as follows. In Section 2 we develop a general framework for automatic non-rigid registration and show that most of the common approaches may be phrased in terms of a variational approach. Furthermore, we introduce the novel curvature based scheme. Section 3 is devoted to numerical aspects of the underlying schemes. In Section 4 we design a fast and direct solver for the linear system associated with the curvature based approach. Finally, in Section 5 we present an application of the curvature registration to MR-mammography images.

2. A unified approach to non-linear registration

Given two images, a reference R and a template T, the aim of image registration is to find a global and/or local transformation from T onto R in such a way that the transformed template matches the reference. To formalize this approach, we assume that the d-dimensional images are represented by the compactly supported mappings $R, T : \Omega \to \mathbb{R}$, where $\Omega :=]0, 1[^d$. In other words, for a particular point $\mathbf{x} \in \Omega$, the quantity $T(\mathbf{x})$ is the intensity or grey value at the spatial position $\mathbf{x}$. Then the purpose of the registration is to determine a displacement field $\mathbf{u} : R^d \to \mathbb{R}^d$ such that $T(\mathbf{x} - \mathbf{u}(\mathbf{x})) = R(\mathbf{x})$ or such that $T(\mathbf{x} - \mathbf{u}(\mathbf{x}))$ is similar to $R(\mathbf{x})$. Whether one is interested in a perfect matching or just an approximate matching depends on the given application, see the examples discussed below. The question then is how to find the desired displacement field $\mathbf{u} = (u_1, \ldots, u_d)$.

Goal of image registration

Registration can be based on a small set of identified points (*landmarks*), see, e.g., [3] or [26], or directly onto measures computed from the image grey values. Here, we are interested in the latter approaches because these are the most flexible schemes. Moreover, the automatic detection of the landmark based on digital image analysis is a sophisticated task. It turns out that most of these schemes may be formulated in terms of a variational approach. To this end we introduce the *joint* functional

$$\mathcal{J}[\mathbf{u}] = \mathcal{D}[R, T; \mathbf{u}] + \alpha \mathcal{S}[\mathbf{u}], \tag{1}$$

where $\mathcal{D}$ represents a *distance measure* (external force) and $\mathcal{S}$ determines the *smoothness* of $\mathbf{u}$ (internal force). The parameter α may be used to control the strength of the smoothness of the displacement versus the similarity of the images. The second term $\mathcal{S}$ is unavoidable. Arbitrary transformations may lead to cracks, foldings, or other unwanted deformations. From a mathematical point of view, $\mathcal{S}$ may also be seen as a regularizing term introduced in order to rule out discontinuous and/or suboptimal solutions.

In the literature one may find various choices for the functional $\mathcal{D}$; cf., e.g., [24]. Probably the most popular choice for the distance measure is provided by the so-called *sum of squared differences* (SSD)

$$\mathcal{D}[R, T; \mathbf{u}] := \frac{1}{2} \|R - T(\cdot - \mathbf{u})\|_{L_2}^2 = \frac{1}{2} \int_\Omega (T(\mathbf{x} - \mathbf{u}(\mathbf{x})) - R(\mathbf{x}))^2 \mathrm{d}\mathbf{x}. \tag{2}$$

For this measure to be successful, one has to assume that the intensities of the two given images are comparable. This assumption restricts this approach to so-called *monomodal* applications, where the images share the same modality, as for example in inter-patient registration. A typical monomodal task is the breast cancer detection. Here, the problem is to match serially acquired MRI's of a female breast before and after a contrast agent injection. The goal is to remove image difference introduced by movement of the patient. However, the registration is tricky task as difference stemming from the contrast agent should be maintained. It should be mentioned that other distance measure are also under consideration, see, e.g. [27].

The SSD distance is suitable for mono-modal registration, i.e. basically images coming from the same source
For multi-modal registration: mutual information may be OK

To relate an area of disfunction to anatomy, it might be necessary to register images of different modalities, for example a PET image to an MR image. A measure which is appropriate for this so-called *multimodal* registration is the so-called *mutual information* which is based on Shannon's entropy, cf., e.g., [35,36] or [8].

In this note, we restrict our attention to the SSD-approach. For a discussion of variational techniques based on mutual information see, e.g., [9].

There exist various choices for the smoothing term $\mathscr{S}$. This is mainly motivated by the fact that particular applications demand for particular properties of the displacement field. Here, we start by briefly outlining four of the most popular choices leading to the *elastic*, *fluid*, *demon*, and *diffusion* registration. Finally, we introduce and discuss the novel *curvature* registration.

2.1. Elastic registration

A smoother motivated by the physics of the underlying object is given by the elastic potential of the displacement field

$$\mathscr{S}^{\text{elas}}[\mathbf{u}] := \int_{\Omega} \frac{\mu}{4} \sum_{j,k=1}^{d} (\partial_{x_j} u_k + \partial_{x_k} u_j)^2 + \frac{\lambda}{2} (\operatorname{div} \mathbf{u})^2 \mathrm{d}\mathbf{x}, \tag{3}$$

where λ and μ are the so-called *Lamé-constants* which do reflect material properties. This smoother was introduced to image registration by Broit [5] and Bajcsy and Kovačič [2]. Image registration based on the SSD-measure $\mathscr{D}$ (2) combined with the regularizer $\mathscr{S}^{\text{elas}}$ is called *elastic matching* or *elastic registration*. A striking example, where one is tempted to look for deformations satisfying elasticity constraints, is the three-dimensional reconstruction of the human brain from a histological sectioning (for details, see [11,28], and references therein).

2.2. Fluid registration

To study and encode patterns of anatomic variability in human populations one needs to quantify local and global shape changes. For example, considerable effort is going into the design of a probabilistic brain atlas, see, for example [7,31–33] or [10].

However, due to its local nature, the linear elasticity model does not allow for large image deformations needed for the mentioned application. Christensen [7] proposed to use instead a viscous fluid model for the deformation. His derivation was based on a specific linearization of the Navier–Stokes equation. Actually, as it turns out, one may obtain Christensen's approach by invoking the elastic potential of the *velocity* $\mathbf{v}$ of the displacement field

$$\mathscr{S}^{\text{fluid}}[\mathbf{u}] := \mathscr{S}^{\text{elas}}[\mathbf{v}], \tag{4}$$

which might be viewed as a visco-elastic model. By introducing an artificial time t, the velocity and the transformation are related via the material derivative

$$\mathbf{v}(\mathbf{x}, t) = \partial_t \mathbf{u}(\mathbf{x}, t) + \nabla \mathbf{u}(\mathbf{x}, t)\mathbf{v}(\mathbf{x}, t). \tag{5}$$

The combination of $\mathscr{D}$ and $\mathscr{S}^{\text{fluid}}[\mathbf{u}]$ is called *fluid matching* or *fluid registration*.

2.3. Demon registration

Christensen's implementation of the fluid registration is based on a SOR type solution scheme for the underlying Euler–Lagrange equations. He reported on many hours of computing time even on a MasPar computer. His time demanding implementation motivated many researchers to search for faster implementations, cf., e.g., [4] or [11,12], or to look for different approaches.

One of the new methods is Thirion's [30] so-called *demon registration*. An option package where roughly speaking, the velocity of the displacement field is computed by smoothing the force field using a Gaussian filter. This elegant idea has reached high popularity, which is due to the fact that its implementation is mainly based on convolution and thus leads to an easy programmable and fast algorithm. However, its convergence behavior is not well understood and needs further investigations. Thirion's technique is used for high dimensional problems or time demanding applications.

2.4. Diffusion registration

As pointed out by Fischer and Modersitzki [12], Thirion's approach may be (partly) considered within the general framework of the functional (1). The key is to introduce the smoother

$$\mathscr{S}^{\text{diff}}[\mathbf{u}] = \frac{1}{2}\sum_{\ell=1}^{d}\int_{\Omega} \|\nabla u_\ell\|^2 \mathrm{d}\mathbf{x}, \tag{6}$$

which has already been used in the area of *optical flow*, cf., e.g., [18]. The resulting scheme is called *diffusion registration*. Its implementation is based on a finite difference approximation of a diffusion like equation and well understood. One of the most interesting features of this method is its speed, see also the comments in Section 4. This makes this scheme very attractive for high-resolution applications.

For example, the registration of three-dimensional MRI's in conjunction with breast cancer surgery.

2.5. Curvature registration

Let us now introduce a new registration technique. It is based on the following smoothing term

$$\mathcal{S}^{\text{curv}}[\mathbf{u}] := \frac{1}{2}\sum_{\ell=1}^{d}\int_{\Omega}(\Delta u_\ell)^2 \mathrm{d}\mathbf{x}. \tag{7}$$

The reason for this particular choice is twofold. The integral might be viewed as an approximation to the curvature of the ℓth component of the displacement field and therefore does penalize oscillations. Most interestingly, by construction $\mathcal{S}^{\text{curv}}$ has a non-trivial kernel containing harmonic functions and in particular affine linear transformations, i.e.,

$$\mathcal{S}^{\text{curv}}[C\mathbf{x}+\mathbf{b}] = 0, \quad \text{for all } C \in \mathbb{R}^{d\times d},\ \mathbf{b} \in \mathbb{R}^d.$$

Thus, in contrast to many other non-linear registration techniques, including the elastic matching, the fluid matching, and the diffusion matching, the new scheme does not require an additional affine linear pre-registration step for being successful.

Note, the smoothing term (7) is very attractive for smoothing optical flow equations as these equations are often dominated by linear movement.

To illustrate the difference between our new curvature based registration and common techniques we present two examples.

Example 1. We compare the performance of the curvature based scheme (7) and the elasticity-driven method (3) for an academic example, where the reference and the template differ by an affine linear transformation.

As the reference image a gray square on a white background positioned in the top left corner is used, whereas the considered template has the very same square rotated by five degrees in the bottom right corner. In other words, an appropriate affine linear transformation would produce a perfect registration result. It turns out, that both the curvature based and the elastic registration lead to a perfect registration, in the sense that the difference between the reference and deformed template vanishes. However, a tracking of the individual pixel reveals that the path towards the optimal registration is completely different. In Fig. 2 the reference (a), template (b), and two intermediate registrations results for the curvature (c,d) as well as for the elastic (e,f) registration are shown. As it is apparent from the figure, the curvature based registration finds the optimal registration result by computing an almost affine linear transformation. In contrast, the displacement computed by the elastic registration scheme is highly non-linear.

Also, this is a striking example for the fact that the similarity between the deformed template and the reference does not necessarily ensure a reliable registration.

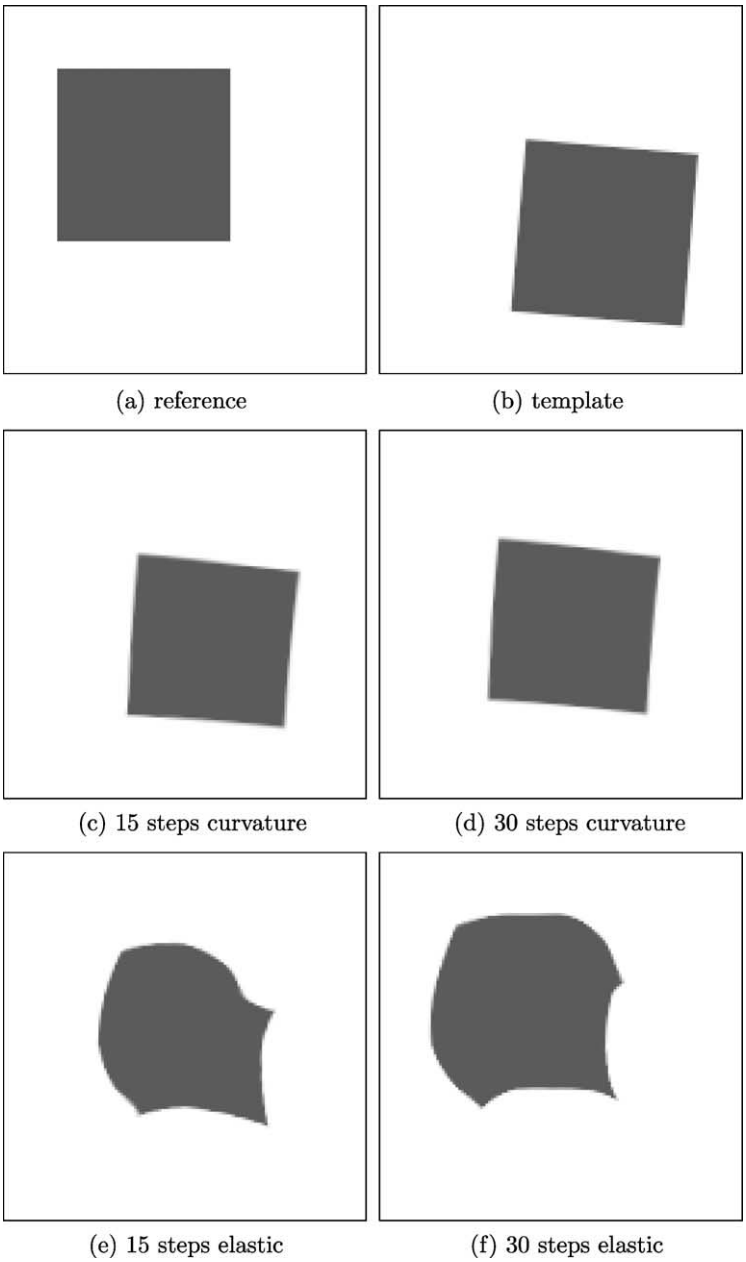

Fig. 2. Reference, template and intermediate registration results; (a) reference, (b) template, (c) after 15 steps of curvature registration, (d) after 30 steps of curvature registration, (e) after 15 steps of elastic registration, and (f) after 15 steps of elastic registration.

Example 2. In Fig. 3 we present registration results for the curvature, diffusion, elastic, and fluid based method, respectively, when applied to two X-rays of a human hand (compare Fig. 1). To compare the respective results, the registration has been stopped for all schemes when the relative error in $\mathscr{D}$ was brought below 60%,

$$\frac{\mathscr{D}[R, T; \mathbf{u}]}{\mathscr{D}[R, T, \mathbf{0}]} \leqslant 0.6.$$

As it is apparent, all four techniques produce nearly the same deformed image $T(\cdot - \mathbf{u})$. However, the displacements, visualized by showing the deformed original uniform grid, are different for the four methods (see, for example, the area around the fingertips).

This example also shows that the selection of the registration technique, for a given application, is not an easy task as the outcome of the different methods is not straightforward to predict.

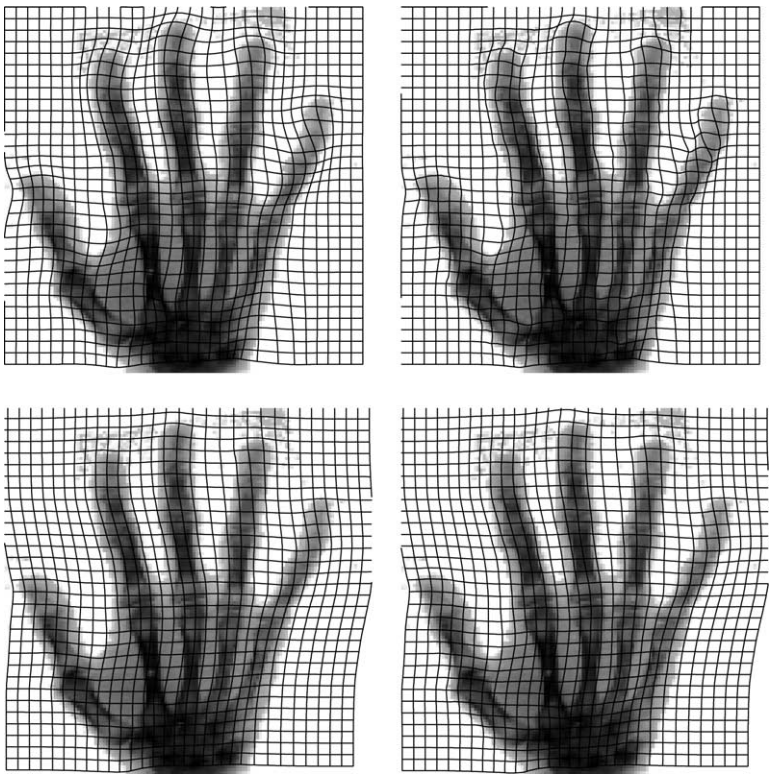

Fig. 3. Template with interpolation grid; top left: after curvature registration, top right: after diffusion registration, bottom left: after elastic registration, and bottom right: after fluid registration.

Fig. 4. Circle deforming into a 'C' for elastic and fluid registration. From left to right: (1) template, (2) reference, (3) patterned deformed template after elastic registration, (4) patterned deformed template after fluid registration.

Example 3. The difference between the elastic and fluid registration in the example above is almost visually indistinguishable. This is due to the fact that for small displacements the velocity and the displacement itself are proportional. To emphasize the difference between these two techniques we present an additional academic example popularized by Christensen. Fig. 4 shows the result of registering a circle to a 'C' for the fluid and elastic registration. To compare the results, both iterations have been stopped after 100 steps. The figure shows that indeed the fluid registration is capable of performing large deformations, while preserving the topology.

3. Numerical treatment of the minimization problem

A variety of different numerical methods for the minimization of the joint functional (1) may be applied. Popular choices include Landwebers iteration, Levenberg–Marquardt like scheme, or multigrid type techniques; cf., e.g., [17].

In this note, we restrict our attention to a variational approach which may be applied to any of the previously discussed registration techniques. In fact, computing the Gâteaux derivative of $\mathscr{J}[\mathbf{u}]$ (cf. (1)) results in the *Euler–Lagrange* equations

$$\mathbf{f}(\mathbf{x}, \mathbf{u}(\mathbf{x})) + \alpha \mathscr{A}[\mathbf{u}](\mathbf{x}) = 0, \quad \mathbf{x} \in \Omega,$$

with

$$\begin{aligned}
\mathscr{A}^{\text{elas}}[\mathbf{u}] &= \mu \Delta \mathbf{u}(\mathbf{x}) + (\lambda + \mu) \nabla \operatorname{div} \mathbf{u}(\mathbf{x}),\\
\mathscr{A}^{\text{fluid}}[\mathbf{u}] &= \mu \Delta \mathbf{v}(\mathbf{x}) + (\lambda + \mu) \nabla \operatorname{div} \mathbf{v}(\mathbf{x}),\\
\mathscr{A}^{\text{diff}}[\mathbf{u}] &= \Delta \mathbf{u},\\
\mathscr{A}^{\text{curv}}[\mathbf{u}] &= \Delta^2 \mathbf{u},
\end{aligned}$$

and

$$\mathbf{f}(\mathbf{x}, \mathbf{u}(\mathbf{x})) = (R(\mathbf{x}) - T(\mathbf{x} - \mathbf{u}(\mathbf{x}))) \cdot \nabla T(\mathbf{x} - \mathbf{u}(\mathbf{x})).$$

These semi-linear partial differential equations provide necessary conditions for $\mathbf{u}$ being a minimizer of (1) and are known as *Navier–Lamé*, *diffusion* and *biharmonic* equation, respectively. The Euler–Lagrange equations for the curvature based registration will be considered in more detail in the next section.

The righthand side $\mathbf{f}$ may be thought off as the driving force for the associated PDE. It is the Gâteaux derivative of the distance measure $\mathscr{D}$. Note, different distance measures would simply lead to different forces but do not alter the type of the PDE.

To solve the PDE's either a fixpoint type iteration scheme

$$\alpha\mathscr{A}[\mathbf{u}^{k+1}](\mathbf{x},t) = -\mathbf{f}(\mathbf{x},\mathbf{u}^k(\mathbf{x},t)), \quad k \geqslant 0,$$

or a time-stepping iteration

We aim to find the steady state solution

$$\partial_t \mathbf{u}^{k+1}(\mathbf{x},t) = \mathbf{f}(\mathbf{x},\mathbf{u}^k(\mathbf{x},t)) + \alpha\mathscr{A}[\mathbf{u}^{k+1}](\mathbf{x},t), \quad k \geqslant 0, \tag{8}$$

with $\mathbf{u}^0 = \mathbf{0}$, is employed. Due to the particular simple geometry of the computational domain $\Omega =]0,1[^d$, typically a finite difference approximation for the derivatives is used. This then leads to high dimensional but rich structured linear systems of equations. These equations have to be solved in each iteration step.

The linear system solve may constitute the most time consuming computational part. Therefore, considerable effort has gone in the development of fast solvers, often accompanied by certain multiresolution techniques like a Gaussian pyramid.

The next section is devoted to the derivation of a fast solution technique for the linear system associated with the curvature based approach.

4. Implementation of curvature registration

In this section we discuss in detail the implementation of the curvature based registration technique. We start by characterizing the minimizer of the associated functional

$$\mathscr{J}[\mathbf{u}] = \mathscr{D}[\mathbf{u}] + \alpha\mathscr{S}^{\text{curv}}[\mathbf{u}], \tag{9}$$

where

$$\mathscr{D}[\mathbf{u}] = \frac{1}{2}\int_\Omega (T(\mathbf{x}-\mathbf{u}(\mathbf{x})) - R(\mathbf{x}))^2 \,\mathrm{d}\mathbf{x},$$

$$\mathscr{S}^{\text{curv}}[\mathbf{u}] = \frac{1}{2}\sum_{\ell=1}^{d}\int_\Omega (\Delta u_\ell)^2 \mathrm{d}\mathbf{x},$$

and Neumann boundary conditions are posed, i.e.,

$$\nabla u_\ell(\mathbf{x}) = \mathbf{0}, \quad \text{for } \mathbf{x} \in \partial\Omega, \quad \ell = 1,\ldots,d. \tag{10}$$

We like to point out, that we do not consider well-posedness of the above continuous formulation, but are more interested in the discretized problem.

The proof of the next theorem is straightforward and can be found in [13].

Theorem 1 (Euler–Lagrange equations). *Let $\mathscr{J}$ be defined by* (9), $R \in L_2(\mathbb{R}^d)$, $T \in C^2(\mathbb{R}^d)$, *and* $\mathbf{u} \in C^4(\Omega)^d$ *fulfilling* (10). *For the perturbation* $\mathbf{v} \in C^2(\Omega)^d$ *fulfilling* (10), *the Gâteaux derivative of $\mathscr{J}$ is given by*

$$\int_\Omega \langle \mathbf{f}(\mathbf{x}, \mathbf{u}(\mathbf{x})) + \alpha \Delta^2 \mathbf{u}, \mathbf{v}(\mathbf{x}) \rangle_{\mathbb{R}^d} \, \mathrm{d}\mathbf{x} = 0, \tag{11}$$

This must hold for each v, then the first argument must vanish

where

$$\mathbf{f}(\mathbf{x}, \mathbf{u}(\mathbf{x})) = (R(\mathbf{x}) - T(\mathbf{x} - \mathbf{u}(\mathbf{x}))) \cdot \nabla T(\mathbf{x} - \mathbf{u}(\mathbf{x})). \tag{12}$$

Our implementation is based on a time marching algorithm for Eq. (8). To begin with, we introduce a time step τ and the uniformly spaced grid points

$$x_{i_1,\ldots,i_d} := \left(\frac{2i_1 - 1}{2n_1}, \ldots, \frac{2i_d - 1}{2n_d} \right) \in \Omega, \quad i_\ell = 1, \ldots, n_\ell, \quad \ell = 1, \ldots, d.$$

These $n := n_1 \cdots n_d$ points are collected in the matrix $X \in \mathbb{R}^{n_1 \times \cdots \times n_d}$. Furthermore, let

Probably, better to say that X belongs to R^(n x d), i.e. the j-th column store the j-th coordinate of all n points

U^k and F^k belong to R^(n x d)
U^k_l and F^k_l belong to R^n

$$U^{(k)} := (U_1^{(k)}, \ldots, U_d^{(k)}), \quad U_\ell^{(k)} := u_\ell(X, k\tau),$$
$$F^{(k)} := (F_1^{(k)}, \ldots, F_d^{(k)}), \quad F_\ell^{(k)} := f_\ell(X, \mathbf{u}(X, k\tau)),$$

$\ell = 1, \ldots, d$. The derivatives are approximated using finite differences, i.e.

$$\mathbf{u}_\ell(X, \tau k) \approx \frac{U_\ell^{(k+1)} - U_\ell^{(k)}}{\tau},$$
$$\Delta^2 \mathbf{u}_\ell(X, \tau k) \approx S^{\mathrm{curv}} * U_\ell^{(k)},$$

where "$*$" denotes the convolution with respect to Neumann boundary conditions,

$$S^{\mathrm{curv}} * V_j = \sum_{q \in \mathcal{N}(j)} S^{\mathrm{curv}}_{j-q} V_q,$$

and $\mathcal{N}(j)$ a neighborhood of j, which depends on the chosen stencil. Here we used the stencil $S^{\mathrm{curv}} = S^{\mathrm{diff}} * S^{\mathrm{diff}}$, where S^{diff} is defined in Table 1. Note that the stencils depend of course on the dimension d. However, we omit this dependency unless it becomes relevant.

Collecting the grid points with respect to a lexicographical ordering in $\vec{X} = (\vec{X}_1^{\mathrm{T}}, \ldots, \vec{X}_d^{\mathrm{T}}) \in \mathbb{R}^N$, where $N := nd$, the discrete analogon to Eq. (8) reads

$$(I_n + \tau\alpha A^{\mathrm{curv}}) \vec{U}_\ell^{(k+1)} = \vec{U}_\ell^{(k)} + \tau \vec{F}_\ell^{(k)}, \quad \ell = 1, \ldots, d, \tag{13}$$

where I_n is the identity matrix and $A^{\mathrm{curv}} = (A^{\mathrm{diff},d})^2$ where $A^{\mathrm{diff},d}$ is defined recursively in the following way. For $p_k \in \{1, 2\}$, $m_k := n_1 \cdots n_k$, and $k = 2, \ldots, d-1$, we have

$$A^{(d-1)}_{p_{d-1},\ldots,p_1} := I_{n_1} \otimes S_{2,p_{d-1},\ldots,p_1} + M_{n_1} \otimes S_{1,p_{d-1},\ldots,p_1} \in \mathbb{R}^{m_1 \times m_1},$$
$$A^{(d-k)}_{p_{d-k},\ldots,p_1} := I_{n_k} \otimes A^{(d-k+1)}_{2,p_{d-k},\ldots,p_1} + M_{n_k} \otimes A^{(d-k+1)}_{1,p_{d-k},\ldots,p_1} \in \mathbb{R}^{m_k \times m_k},$$
$$A^{\mathrm{diff},d} := I_{n_d} \otimes A_2^{(1)} + M_{n_d} \otimes A_1^{(1)} \in \mathbb{R}^{m_d \times m_d},$$

Table 1
Matrix stencils for the discrete Laplace operator

$$S^{\mathrm{diff},d}_{n_1,\ldots,n_d} = \begin{cases} -2d, & n_\ell = 2,\ \ell = 1,\ldots,d \\ 1, & n_j = 1,3,\ n_\ell = 2,\ \ell = 1,\ldots,d,\ \ell \neq j \end{cases}$$

$$S^{\mathrm{diff},2} = \begin{pmatrix} 0 & 1 & 0 \\ 1 & -4 & 1 \\ 0 & 1 & 0 \end{pmatrix}, \quad S^{\mathrm{diff},3}_{:,:,1} = \begin{pmatrix} 0 & 0 & 0 \\ 0 & 1 & 0 \\ 0 & 0 & 0 \end{pmatrix}$$

$$S^{\mathrm{diff},3}_{:,:,2} = \begin{pmatrix} 0 & 1 & 0 \\ 1 & -6 & 1 \\ 0 & 1 & 0 \end{pmatrix}, \quad S^{\mathrm{diff},3}_{:,:,3} = \begin{pmatrix} 0 & 0 & 0 \\ 0 & 1 & 0 \\ 0 & 0 & 0 \end{pmatrix}$$

where

$$M_m := \begin{pmatrix} 1 & 1 & & & \\ 1 & 0 & 1 & & \\ & \ddots & \ddots & \ddots & \\ & & 1 & 0 & 1 \\ & & & 1 & 1 \end{pmatrix} \in \mathbb{R}^{m\times m}. \tag{14}$$

In particular for $d = 2$, we have

$$A^{(1)}_p = I_{n_1} \otimes S_{2,p} + M_{n_1} \otimes S_{1,p}, \quad p = 1,2,$$
$$A^{\mathrm{diff},2} = I_{n_2} \otimes A^{(1)}_2 + M_{n_2} \otimes A^{(1)}_1,$$

and for $d = 3$, we have

$$A^{(2)}_{p,q} = I_{n_1} \otimes S_{2,p,q} + M_{n_1} \otimes S_{1,p,q}, \quad p,q = 1,2,$$
$$A^{(1)}_q = I_{n_2} \otimes A^{(2)}_{2,q} + M_{n_2} \otimes A^{(2)}_{1,q}, \quad q = 1,2,$$
$$A^{\mathrm{diff},3} = I_{n_2} \otimes A^{(1)}_2 + M_{n_3} \otimes A^{(1)}_1.$$

An eigendecomposition of A^{diff} and A^{curv} is based on the factorization of M_m and the recursive structure of the matrices. With

$$C_m := \left(\cos\frac{(2j+1)k\pi}{2m}\right)_{j,k=0,\ldots,m-1} \in \mathbb{R}^{m\times m}, \tag{15}$$

$$V_m := C_m \mathrm{diag}\left(\sqrt{1/m}, \sqrt{2/m}, \ldots, \sqrt{2/m}\right) \in \mathbb{R}^{m\times m}, \tag{16}$$

$$D_m := 2\ \mathrm{diag}\left(\cos\frac{k\pi}{m},\ k = 0,\ldots,m-1\right) \in \mathbb{R}^{m\times m}, \tag{17}$$

the following lemma can be shown; cf., e.g., [29] or [23].

Lemma 1. *Let $M_m \in \mathbb{R}^{m\times m}$ be as in* (14) *and C_m, V_m, and D_m be as in* (15)–(17), *respectively. Then it holds*

1. $M_m V_m = V_m D_m$ *and* $V_m^{\mathrm{T}} V_m = I_m$.
2. *Let S be any d-dimensional, symmetric matrix stencil and $A^{\mathrm{diff},d}$ be the matrix representation of the convolution with S with respect to Neumann boundary conditions. Then*

$$\begin{aligned} D^{\mathrm{diff},d} &:= (V_{n_d} \otimes \cdots \otimes V_{n_1})^{\mathrm{T}} A^{\mathrm{diff},d} \, (V_{n_d} \otimes \cdots \otimes V_{n_1}) \\ &= \mathrm{diag}(d_{j_1,\ldots,j_d},\ j_q = 1,\ldots,n_1,\ q = 1,\ldots,d), \end{aligned}$$

where $d_{j_1,\ldots,j_d}$ is defined recursively by

$$\begin{aligned} d_{j_1}^{p_{d-1},\ldots,p_1} &= S_{2,p_{d-1},\ldots,p_1} + 2S_{2,p_{d-1},\ldots,p_1} \cos\frac{j_1\pi}{n_1}, \\ d_{j_1,\ldots,j_k}^{p_{d-k},\ldots,p_1} &= d_{j_1,\ldots,j_k}^{2,p_{d-k},\ldots,p_1} + 2d_{j_1,\ldots,j_k}^{1,p_{d-k},\ldots,p_1} \cos\frac{j_k\pi}{n_k}, \\ d_{j_1,\ldots,j_d} &= d_{j_1,\ldots,j_{d-1}}^{2} + 2d_{j_1,\ldots,j_{d-1}}^{1} \cos\frac{j_d\pi}{n_d}. \end{aligned}$$

The next corollary simplifies the previous lemma for dimension $d = 2, 3$ and the particular matrix stencil given in Table 1.

Corollary 1. *Let $A^{\mathrm{diff},d}$ be the matrices associated with $S^{\mathrm{diff},d}$, cf. Table* 1. *Then we have*

$$\begin{aligned} D^{\mathrm{diff},2} &:= (V_{n_2} \otimes V_{n_1})^{\mathrm{T}} A^{\mathrm{diff},2} (V_{n_2} \otimes V_{n_1}) \\ &= \mathrm{diag}(d_{j_1,j_2},\ j_1 = 1,\ldots,n_1,\ j_2 = 1,\ldots,n_2), \\ D^{\mathrm{diff},3} &:= (V_{n_3} \otimes V_{n_2} \otimes V_{n_1})^{\mathrm{T}} A^{\mathrm{diff},3} (V_{n_3} \otimes V_{n_2} \otimes V_{n_1}) \\ &= \mathrm{diag}(d_{j_1,j_2,j_3},\ j_\ell = 1,\ldots,n_\ell,\ \ell = 1,2,3), \end{aligned}$$

where

$$\begin{aligned} d_{j_1,j_2} &= -4 + 2\cos\frac{(j_1-1)\pi}{n_1} + 2\cos\frac{(j_2-1)\pi}{n_2}, \\ d_{j_1,j_2,j_3} &= -6 + 2\cos\frac{(j_1-1)\pi}{n_1} + 2\cos\frac{(j_2-1)\pi}{n_2} + 2\cos\frac{(j_3-1)\pi}{n_3}, \end{aligned}$$

and $j_\ell = 1,\ldots,n_\ell$, $\ell = 1,2,3$.

Lemma 1 enables one to explicitly diagonalize the coefficient matrix in (13),

$$(V_{n_d} \otimes \cdots \otimes V_{n_1})^{\mathrm{T}} (I_n + \tau\alpha A^{\mathrm{curv}})(V_{n_d} \otimes \cdots \otimes V_{n_1}) = I_n + \tau\alpha (D^{\mathrm{diff}})^2.$$

Table 2
DCT based implementation of curvature registration

Choose $\tau > 0$, initialize $k = 0$, X, $U^{(k)} = 0$.
For $k = 0, \ldots,$
  % Compute forces
  $F_\ell^{(k)} = (T(X - U^{(k)}) - R(X))\, \partial_{x_\ell} T(X - U^{(k)})$
  % Solve linear system
  For $\ell = 1, \ldots, d$,
    $G = \mathrm{DCT}(U_\ell^{(k)} + \tau F_\ell^{(k)})$
    For $p = 1, \ldots, d, \quad j_p = 1, \ldots, n_p$,
      $V_{j_1,\ldots,j_p} = G_{j_1,\ldots,j_p}[1 + \tau\alpha d^2_{j_1,\ldots,j_p}]^{-1}$,
    end,
    $U_\ell^{(k+1)} = \mathrm{DCT}^{-1}(V)$,
  end,
end.

Hence, the linear solve reduces to the multiplication by the above Kronecker products followed by a multiplication by a diagonal matrix. This may be efficiently realized by a discrete cosine transform resulting in a fast $\mathcal{O}(n \log n)$ implementation. The overall algorithm is summarized in Table 2.

It is worth noticing that a similar factorization may be applied to the linear system associated with the diffusion registration. However, by exploiting an additive operator splitting scheme, one may even come up with an $\mathcal{O}(n)$ implementation (for details, see [12]).

5. Experiments

To illustrate the performance of the new approach we present the registration of two clinical 2D magnet-resonance (MR) images of a female breast.

Fig. 5 displays a so-called low-resolution MR-scan (256×256) from the wash-in phase of a contrast agent and a high-resolution MR-scan (512×512) taken between the wash-in and wash-out phase. Note that the white spot in upper part of the images displays a tumor while the white spot in the lower part is related to scanning artifacts.

The overall goal of the joint project is to study the dynamic behavior of the contrast agent in detail. This problem will be presented in a forthcoming paper. In this note, however, we would like to demonstrate that our new approach is capable of dealing with images which initially had different resolutions and different intensity ranges.

Fig. 5 displays the convergence curve as well as the difference images before and after registration. Note that the convergence behavior is rather smooth and that the difference has been reduced by about 40%. To be precise, we haven chosen for our

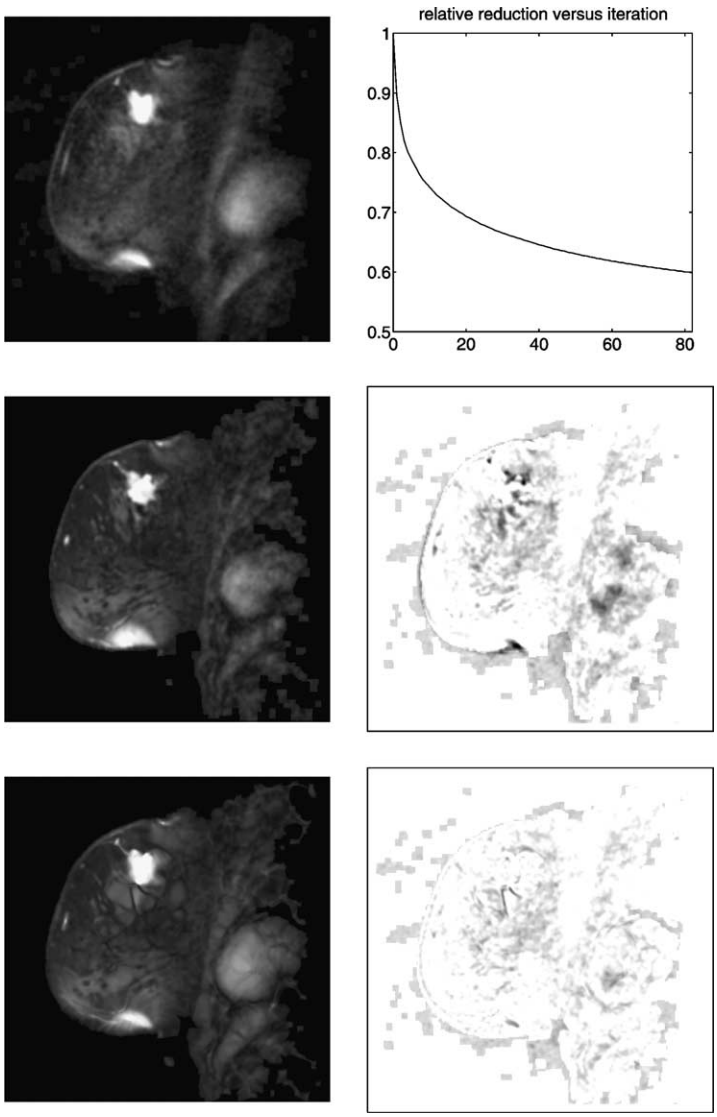

Fig. 5. Top: reference R (preprocessed section #18 from the wash-in phase 18); middle left: template T (preprocessed section #36 from a high-resolution image taken at optimal time-point); middle right: difference before registration, $|R - T| = 100\%$; bottom left: template $\hat{T}$ after registration; bottom right: difference after registration, $|R - \hat{T}| \approx 60\%$; top right: relative distance $|R - T_k|/|R - T|$ versus iteration.

computation the parameter $\alpha = 0.01$ and $\tau = 100$. The iteration was stopped when the relative error was below 10^{-4}, which happened after 80 iterations.

Acknowledgment

We are indebted to Bruce L. Daniel (Department of Radiology, Stanford University) for providing the breast MR images and various discussions. We also thank the anonymous referees for helpful comments.

References

[1] Y. Amit, A nonlinear variational problem for image matching, SIAM J. Sci. Comput. 15 (1) (1994) 207–224.
[2] R. Bajcsy, S. Kovačič, Multiresolution elastic matching, Comput. Vision, Graphics Image Process. 46 (1989) 1–21.
[3] F.L. Bookstein, Principal warps: thin-plate splines and the decomposition of deformations, IEEE Trans. Patttern Anal. Mach. Intell. 11 (6) (1989) 567–585.
[4] M. Bro-Nielsen, C. Gramkow, Fast fluid registration of medical images, in: Lecture Notes in Computer Science, vol. 1131, 1996, pp. 267–276.
[5] C. Broit, Optimal registration of deformed images, Ph.D. Thesis, Computer and Information Science, University of Pennsylvania, 1981.
[6] L.G. Brown, A survey of image registration techniques, ACM Comput. Surveys 24 (4) (1992) 325–376.
[7] G.E. Christensen, Deformable shape models for anatomy, Ph.D. Thesis, Sever Institute of Technology, Washington University, 1994.
[8] A. Collignon, F. Maes, D. Delaere, D. Vandermeulen, P. Seutens, G. Maral, Automatic multimodality image registration using information theory, in: Information Processing Medical Imaging: Proceedings of 14th International Conference IPMI'95, 1995, pp. 263–274.
[9] E. D'Agostino, J. Modersitzki, F. Maes, D. Vandermeulen, B. Fischer, P. Suetens, Free-form registration using mutual information and curvature regularization, Preprint A-03-05, Institute of Mathematics, University of Lübeck, 2003.
[10] B.M. Dawant, S.L. Hartmann, S. Gadamsetty, Brain atlas deformation in the presence of large space-occupying lesions, in: C. Taylor, A. Colchester (Eds.), Medical Image Computing and Computer-Assisted Intervention, MICCAI'99, LNCS, vol. 1679, 1999, pp. 589–596.
[11] B. Fischer, J. Modersitzki, Fast inversion of matrices arising in image processing, Numer. Algorithms 22 (1999) 1–11.
[12] B. Fischer, J. Modersitzki, Fast diffusion registration, in: AMS Contemporary Mathematics, Inverse Problems, Image Analysis, and Medical Imaging 313 (2002) 117–129.
[13] B. Fischer, J. Modersitzki, Curvature based image registration, JMIV 18 (1) (2003) 81–85.
[14] B. Fischer, J. Modersitzki, Combination of automatic non-rigid and landmark based registration: the best of both worlds, in: M. Sonka, J.M. Fitzpatrick (Eds.), Medical Imaging 2003: Image Processing, Proc. SPIE, vol. 5032, 2003, pp. 1037–1048.
[15] B. Fischer, J. Modersitzki, FLIRT: A Flexible Image Registration Toolbox, in: J.C. Gee, J.B.A. Maintz, M.W. Vannier (Eds.), Biomedical Image Registration, Second International Workshop, WBIR 2003, LCNS, vol. 2717, Springer, Berlin, 2003, pp. 261–270.
[16] S. Haker, A. Tannenbaum, R. Kikinis, Mass preserving mappings and image registration, in: MICCAI 2001, LNCS, vol. 2208, 2001, pp. 120–127.
[17] S. Henn, K. Witsch, A multigrid approach for minimizing a nonlinear functional for digital image matching, Computing 64 (4) (1999) 339–348.
[18] B.K.P. Horn, B.G. Schunck, Determining optical flow, Artificial Intell. 17 (1981) 185–204.
[19] M. Lefébure, L.D. Cohen, Image registration, optical flow and local rigidity, JMIV 14 (2) (2001) 131–147.

[20] J.B.A. Maintz, M.A. Viergever, A survey of medical image registration, Medical Image Anal. 2 (1) (1998) 1–36.
[21] C.R. Maurer, J.M. Fitzpatrick, Interactive image-guided neurosurgery, in: A Review of Medical Image Registration, American Association of Neurological Surgeons, Park Ridge, IL, 1993, pp. 17–44.
[22] M.I. Miller, L. Younes, Group actions, homeomorphisms, and matching: a general framework, Int. J. Comput. Vision 41 (1/2) (2001) 61–84.
[23] D. Potts, G. Steidl, Optimal trigonometric preconditioners for nonsymmetric Toeplitz systems, Linear Algebra Appl. 281 (1998) 265–292.
[24] A. Roche, Recalage d'images médicales par inférence statistique, Ph.D. Thesis, Université de Nice, Sophia-Antipolis, France, 2001.
[25] T. Rohlfing, C.R. Maurer Jr., Volume-preserving non-rigid registration of MR breast images using free-form deformation with an incompressibility constraint, IEEE TMI 22 (6) (2003) 730–741.
[26] K. Rohr, Landmark-based image analysis, in: Computational Imaging and Vision, Kluwer Academic Publishers, Dordrecht, 2001.
[27] D. Rueckert, L.I. Sonoda, C. Hayes, D.L.G. Hill, M.O. Leach, D.J. Hawkes, Nonrigid registration using free-form deformations: applications to breast MR images, IEEE TMI 18 (8) (1999) 712–721.
[28] O. Schmitt, Die multimodale Architektonik des menschlichen Gehirns, Habilitation, Insitute of Anatomy, Medical University of Lübeck, Germany, 2001.
[29] G. Strang, The discrete cosine transform, SIAM Rev. 41 (8) (1999) 135–147.
[30] J.-P. Thirion, Image matching as a diffusion process: an analogy with Maxwell's demons, Med. Image Anal. 2 (3) (1998) 243–260.
[31] A.W. Toga, Three-Dimensional Neuroimaging, Raven Press, New York, 1990.
[32] A.W. Toga, Brain Warping, Academic Press, San Diego, 1999.
[33] A.W. Toga, J.C. Mazziota, Brain Mapping, Academic Press, San Diego, 1996.
[34] P.A. van den Elsen, E.-J.D. Pol, M.A. Viergever, Medical image matching—a review with classification, IEEE Eng. Med. Biol. (1993) 26–38.
[35] P.A. Viola, W.M. Wells III, Alignment by maximization of mutual information, in: Fifth International Conference on Computer Vision, IEEE, 1995, pp. 16–23.
[36] P.A. Viola, Alignment by maximization of mutual information, Ph.D. Thesis, Massachusetts Institute of Technology, 1995, pp. 1–155.